DOI: https://doi.org/10.20372/star.V14.i1.02
ISSN: 2226-7522 (Print) and 2305-3372 (Online)
Science, Technology and Arts Research Journal
Sci. Technol. Arts Res. J., Jan. – March 2025, 14(1), 11-18
Journal Homepage: https://journals.wgu.edu.et
Original Research

Structural and Ferroelectric characteristics of (1-x) $NaNbO_3$-x$(Bi_{0.5}Li_{0.5})TiO_3$ lead-free electro-ceramic material

Kebede Legesse
Department of Physics, College of Natural and Computational Sciences, Wollega University, Nekemte, Ethiopia

Abstract

To investigate its structure and ferroelectric properties, a sodium niobate-bismuth lithium titanate ((1-x)$NaNbO_3$-x$(Bi_{0.5}Li_{0.5})TiO_3$) ceramic with a composition of x = 0.05 was created using a solid-state mixed oxide reaction method. Na_2CO_3, Nb_2O_5, Li_2CO_3, Bi_2O_3, and TiO_2 were used to make the composite. The ((1-x) $NaNbO_3$-x$(Bi_{0.5}Li_{0.5})TiO_3$) (x = 0.05) exhibits an orthorhombic crystal structure based on the X-ray diffraction pattern. The X-ray diffraction research was measured using an X-ray diffractometer. The morphological inspection is analysed using a scanning electron microscope (SEM). Ferroelectric measurements were performed using the P-E loop tracer. The coercive field (Ec) and remnant polarisation (Pr) of the ceramic sample were observed to rise with increasing applied voltage. Critical evidence from the combined structure and hysteresis loop analysis suggests that the ((1-x)$NaNbO_3$-x$(Bi_{0.5}Li_{0.5})TiO_3$) (x = 0.05) ceramic is expected to be a potential new lead-free electronic material contender. Hence, ferroelectric materials have many applications, including *capacitors, non-volatile memory, piezoelectric for ultrasound imaging and actuators, electro-optic materials for data storage applications, and thermistors.*

Article Information

Article History:
Received: 24-09-2024
Revised: 26-11-2024
Accepted: 29-12-2024

Keywords:
Ferroelectric property, Structure, $NaNbO_3$, $(Bi_{0.5}Li_{0.5})TiO_3$, $NaNbO_3$ -$Bi_{0.5}Li_{0.5})TiO_3$

*Corresponding Author:
Kebede Legesse
E-mail:
kebedelg@wollegauniversity.edu.et

INTRODUCTION

Ferroelectric materials offer a wide range of advantageous properties for the electronics industry. Ferroelectric ceramics were originally reported in 1920 after Valasek discovered ferroelectricity occurrences in Seignette or Rochell Salt (Molak & Pawełczy, 2009). These salts were shown to exhibit polarisation hysteresis and phase transitions from the polar to the non-polar phase. Single crystals of ferroelectric sodium niobate have been studied using X-ray diffraction. The unit cell has orthorhombic dimensions. One extremely unexpected feature of the structure is that the niobium ions are shifted 0.11 Å in opposite directions down the axis from their distinct places in the ideal perovskite structure (Kruczek et al., 2006). Contrary to the commonly held belief that this type of ferroelectric material spontaneously polarises, the nonpolar structure results from this axis

being equivalent to the polar axis in orthorhombic $BaTiO_3$. Any pseudo-symmetrical chemical's space group and unit-cell size can be described by examining the elements that determine its space group in general (Lente & de Los Guerra, 2004). Similar orthorhombic distortion with atom displacements occurs in various other non-ferroelectric perovskite-type compounds when the atoms are not packed appropriately. Given that the displacements in $NaNbO_3$ can be described by a comparable misfit of the atomic radii in the structure, this suggests that the orthorhombic distortion brought on by the ferroelectricity would lower the energy associated with these displacements. The shifts cannot be entirely explained by these packing variables alone, but they can be explained if the oxygen and niobium atoms additionally have a sizable amount of homopolar bonding (Shiratori & Magrez, 2007, Mishra & Choudhury, 2007).

Due to global industrialisation and population growth, energy consumption has increased significantly in recent years. This has increased the demand for energy storage devices to compensate for the disruption of renewable energy sources (Smiga & Garbarz-Glos, 2008; Smiga et al., 2008). Given the limited resources and environmental concerns, lead-free energy storage and dielectric materials must be developed. It is well recognised that a material's composition, structure, and experimental setup all affect its dielectric properties. Dielectric ceramic capacitors have garnered a lot of attention recently because of their rapid rates of charge and discharge, which has led to their immense potential in the pulse power supply sector.

However, its potential for downsizing and mobility has been severely limited due to its low energy density. Strong electric polarisation, large breakdown strength, low remnant polarisation, and large discharge current density are all highly needed in order to enhance the energy storage performance of dielectric ceramic capacitors (Morita, 2010; Xu & Jiang, 2009; Qiu et al., 2007). Dielectric energy storage performance can be improved through chemical alteration. For example, introducing bismuth-containing compounds to certain dielectric materials may activate or augment their relaxor capabilities.

Therefore, it is essential to find a practical way to incorporate a compound based on $(Bi_{0.5}Li_{0.5})\ TiO_3$ in order to obtain satisfactory complete energy storage performance. In this work, we study the ferroelectric behaviour of the (1-x) $NaNbO_3$-x$(Bi_{0.5}Li_{0.5})TiO_3$ composite nanopowder ceramic compound (x = 0.05) (Selbach & Tybell, 2007; Chaudhari & Bichile, 2010).

MATERIALS AND METHODS

The (1-x) $NaNbO_3$-x$(Bi_{0.5}Li_{0.5})\ TiO_3$ (x = 0.05) composites are made by the conventional solid-state method. TiO_2, Bi_2O_3, Li_2CO_3, Nb_2O_5, and Na_2CO_3 are the components used to make the composite. All components combined in a stoichiometric ratio are processed for 12 hours to create a fine powder using an agate motor. This powdered substance is calcined in a furnace at 850°C for 12 hours. A gel that is made by mixing 5% PVC (polyvinyl alcohol) with calcined material is ground into a fine powder. This fine powder is put through a screen and compressed into pellets using a hydraulic press. This pellet is sintered in a furnace at 900°C for 16 hours. Flat surfaces were polished for the electrical measurement, and silver paste electrodes were dried under a

lamp for forty minutes to remove any remaining moisture. The prepared sample was characterised using the following techniques. The X-ray diffraction investigations were measured using an X-ray diffractometer. The morphological study is evaluated using a scanning electron microscope (SEM). Ferroelectric measurements were performed using the P-E loop tracer. Because the electric field causes a little shift in the charge balance within the material, the dielectric system in ferroelectric materials develops an electrical dipole moment. Dipole moment per unit volume, which is proportional to the electric field, is the definition of polarisation. The polarisation P of a polarised substance is the amount of dipole moment μ per unit volume V (Teixeira et al., 2012).

$$P = \frac{\mu}{V} \quad (1)$$

$$\mu = Qd \quad (2)$$

Where d is the vector that represents the distance between the charges, Q is the charge magnitude, and μ is the dipole moment vector. The applied field and the polarisation are always proportionate. Consequently, it can be expressed as follows:

$$P = \varepsilon_o \chi_e E \quad (3)$$

According to Moreira et al. (2008) and de Moura et al. (2010), the dielectric susceptibility, or χ_e, is a unitless constant that characterises the dielectric's capacity to generate dipoles. The polarisation will be as follows since the dielectric susceptibility χe equals (ε_r-1), where ε_r is the relative permittivity:

$$P = \varepsilon_o E(\varepsilon_r - 1) \quad (4)$$

Results and Discussions

Figure 1 shows the XRD pattern of the (1-x) $NaNbO_3$-x($Bi_{0.5}Li_{0.5}$)TiO_3(x= 0.05) composite, which was recorded in the 30–80° range. The XRD pattern confirms the single-phase orthorhombic structure.

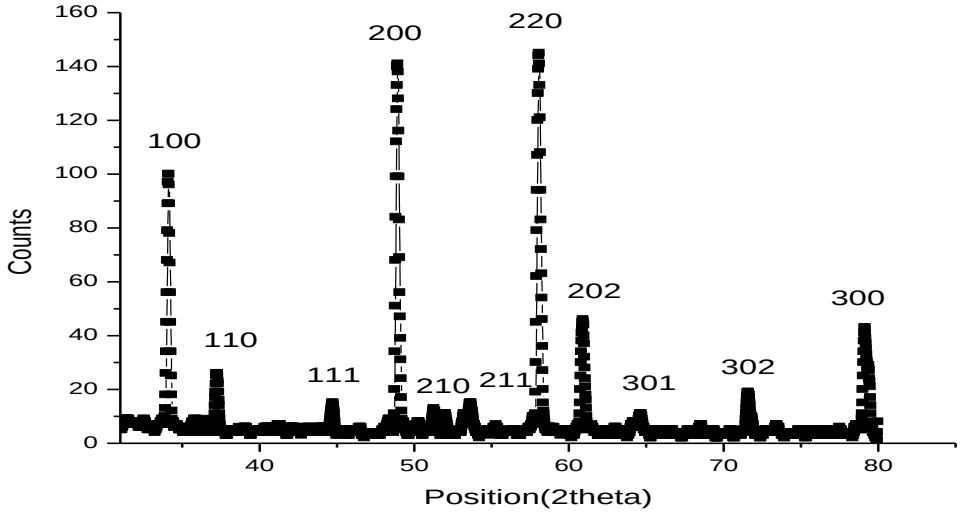

Figure 1. *XRD pattern of (1-x) $NaNbO_3$-x($Bi_{0.5}Li_{0.5}$)TiO_3 (x = 0.05) ceramic*

Since there are no further peaks linked to impurities in Figure 1, the composite has a highly crystalline nature (Volanti et al., 2010; Satapathy & Wadhawan, 2005). The solid-

state reaction's well-defined powder peak in the XRD pattern indicates that these materials have excellent crystallinity.

Table 1

Structure, crystallite size and density of (1-x) $NaNbO_3$-x($Bi_{0.5}Li_{0.5}$) TiO_3 (x = 0.05) Nano powder ceramic

Compositions	Structure	Lattice Parameters (A°)	Relative Density (%)	Porosity %	Crystallite size (nm)	Average grain size
0.05	orthorhombic	A = 4.44 b = 5.07 c = 5.57	95.13	4.87	12.25	2.21

The composite micrographs are shown in Figure 2. It shows that the lines separating two nearby sections are evident and that the micrograph has a dense microstructure. The grain size of the composite is shown in Table 1. The surface of the sample seems to be smooth. The sample contains small cavities. The sample shows clear grain that is separated by grain boundaries.

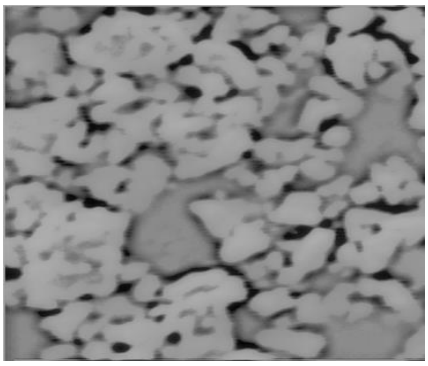

Figure 2. *SEM micrographs of (1-x) $NaNbO_3$-x($Bi_{0.5}Li_{0.5}$) TiO_3 (x = 0.05) ceramic*

When the solid-state reaction mechanism, direction, and synthesis method are used to create the ceramic nanopowder sample (1-x) $NaNbO_3$-x($Bi_{0.5}Li_{0.5}$) TiO_3 (x = 0.05), the hysteresis loop is shown in Figure 3. One feature of ferroelectricity is the hysteresis loop. The P–E hysteresis loops from polarization to the electric field at room temperature under various applied fields were used to investigate the ferroelectric behaviour of (1-x) $NaNbO_3$-x($Bi_{0.5}Li_{0.5}$) TiO_3 (x = 0.05) ceramic. At ambient temperature, the ferroelectric hysteresis loop is depicted in Figure 3. Table 2 showed that spontaneous

polarization, remnant polarization, and coercive electric field were present at room temperature, indicating that they might be used as switching devices. It has been noted that when the applied voltage increases, so does the loop area. As the applied voltage increases, so does the coercive field (EC) and remnant polarization (Pr). Hysteresis tests were conducted at 11kv/cm and 12kv/cm to examine the impact of spatial charges on ferroelectric effects since the contribution of spatial charges is noticeable at low frequencies.

The solid-state synthesis method yields a powder with a remanent polarization (Pr) of 0.35μC/cm^2 and a typical ferroelectric material loop. For 12kv/cm, 0.28μC/cm^2 is revealed, compared to 11kv/cm generated utilizing the solid-state synthesis technique. We believe that the morphological influence obtained by the solid-state synthesis method is responsible for the lower defect concentration on (1-x) $NaNbO_3$-x($Bi_{0.5}Li_{0.5}$) TiO_3 (x = 0.05) powder, which can be linked to the spatial charges' contribution for ferroelectric effect (Milanez & Figueiredo, 2009).

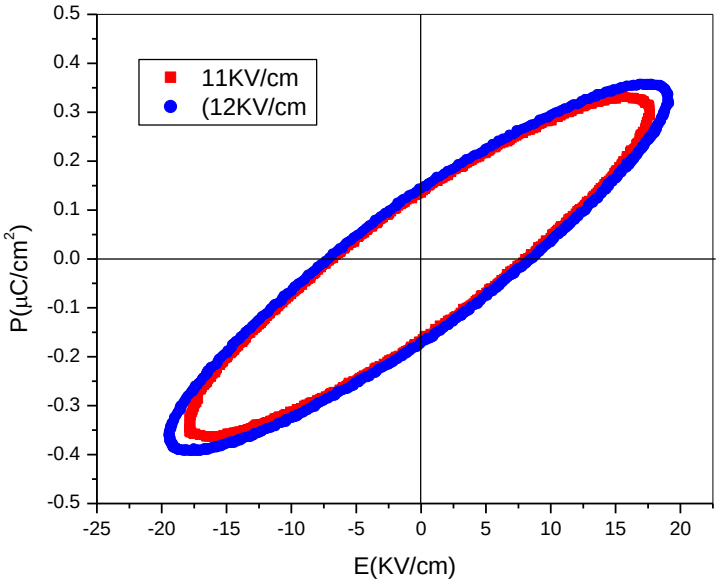

Figure 3. *Hysteresis loop plot at RT for (1-x) $NaNbO_3$-x($Bi_{0.5}Li_{0.5}$)TiO_3 (x = 0.05) ceramic*

The ferroelectric loop of the (1-x) $NaNbO_3$-x($Bi_{0.5}Li_{0.5}$) TiO_3 sample shows a notable energy loss. At an applied voltage of 12 kV, the maximum values of Ps, Pr, and EC for a composition of 0.05 were 0.35μC/cm^2, 0.51μC/cm^2, and 13.7kV/cm. Because of the testing apparatus's narrow range, the ceramic generally displayed well-developed, unsaturated hysteresis loops. It was therefore determined that the (1-x) $NaNbO_3$-x ($Bi_{0.5}Li_{0.5}$)TiO_3 sample (x = 0.05) was ferroelectric.

Table 2

Saturation polarization & remnant polarization values at room temperature of (1-x) $NaNbO_3$-x($Bi_{0.5}Li_{0.5}$)TiO_3 (x = 0.05) Nano powder ceramic

Applied Voltage	Saturation Polarisation	Coercive Field	Remnant Polarisation
11KV/cm	0.44 μC/cm^2	12.57KV/cm	0.28 μC/cm^2
12KV/cm	0.51 μC/cm^2	13.78KV/cm	0.35 μC/cm^2

CONCLUSIONS

The solid-state reaction pathway approach and the precursors TiO_2, Bi_2O_3, Li_2CO_3, and Nb_2O_5 were used in this study to successfully generate an electroceramics nanopowder (1-x) $NaNbO_3$-x ($Bi_{0.5}Li_{0.5}$) TiO_3 (x = 0.05). Investigating the ferroelectric properties and structural implications of (1-x) $NaNbO_3$-x($Bi_{0.5}Li_{0.5}$) TiO_3 (x = 0.05) was the goal of the current work. The crystal structure of the ceramic was found to be orthorhombic by this investigation. The microstructure of the micrograph is thick, and it is easy to identify the boundaries between two neighbouring sections. The development of spherical hysteresis loops indicates that powders produced using the solid-state method are more affected by spatial charges.

Recommendations

The polarization characteristics of the sample are affected by an increase in voltage at a constant temperature. To ensure that the test material is suitable for application and provides adequate information about the ferroelectric properties, more research on the test material with a greater variety of compositions and ac-biased fields is required.

CRediT authorship contribution statement

The author confirms the sole responsibility for the conception of the study, presented results, and manuscript preparation.

Declaration of Competing Interest

The author declares that there is no conflict of interest.

Data availability

The data used in this research is available upon request.

Acknowledgments

For providing the required assistance, the author would like to thank the Department of Physics, Wollega University.

REFERENCES

Chaudhari, V. A., & Bichile, G. K. (2010). Structural and impedance spectroscopic studies on PbZrxTi1− xO3 ceramics. *Physica B: Condensed Matter*, *405*(2), 534-539. https://doi.org/10.1016/j.physb.2009.09.060

De Moura, A., Lima, R., Moreira, M., Volanti, D., Espinosa, J., Orlandi, M., Pizani, P., Varela, J., & Longo, E. (2010). ZnO architectures synthesized by a microwave-assisted hydrothermal method and their photoluminescence properties. *Solid State*

Ionics, *181*(15–16), 775–780. https://doi.org/10.1016/j.ssi.2010.03.013

Kruczek, M., Talik, E., & Kania, A. (2006). Electronic structure of AgNbO3 and NaNbO3 studied by X-ray photoelectron spectroscopy. *Solid State Communications*, *137*(9), 469–473. https://doi.org/10.1016/j.ssc.2006.01.001

Lente, M., Guerra, J. L. S., Eiras, J., & Lanfredi, S. (2004). Investigation of microwave dielectric relaxation process in the antiferroelectric phase of NaNbO3 ceramics. *Solid State Communications*, *131*(5), 279–282. https://doi.org/10.1016/j.ssc.2004.05.035

Milanez, J., De Figueiredo, A. T., De Lazaro, S., Longo, V. M., Erlo, R., Mastelaro, V. R., Franco, R. W. A., Longo, E., & Varela, J. A. (2009). The role of oxygen vacancy in the photoluminescence property at room temperature of the CaTiO3. *Journal of Applied Physics*, *106*(4). https://doi.org/10.1063/1.3190524

Mishra, S. K., Choudhury, N., Chaplot, S. L., Krishna, P. S. R., & Mittal, R. (2007). Competing antiferroelectric and ferroelectric interactions inNaNbO3: Neutron diffraction and theoretical studies. *Physical Review B*, *76*(2). https://doi.org/10.1103/physrevb.76.024110

Molak, A., Pawełczyk, M., Kubacki, J., & Szot, K. (2009). Nano-scale chemical and structural segregation induced in surface layer of NaNbO3 crystals with thermal treatment at oxidising conditions studied by XPS, AFM, XRD, and electric properties tests. *Phase Transitions*, *82*(9), 662-682. https://doi.org/10.1080/01411590903341155

Moreira, M. L., Mambrini, G. P., Volanti, D. P., Leite, E. R., Orlandi, M. O., Pizani, P. S., & Varela, J. A. (2008). Hydrothermal microwave: a new route to obtain photoluminescent crystalline BaTiO3 nanoparticles. *Chemistry of Materials*, *20*(16), 5381-5387. https://doi.org/10.1021/cm801638d

Morita, T. (2010). Piezoelectric materials synthesized by the hydrothermal method and their applications. *Materials*, *3*(12), 5236-5245. https://doi.org/10.3390/ma3125236

Qiu, S., Fan, H., & Zheng, X. (2006). Pb(Zr0.95Ti0.05)O3 powders synthesized by Pechini method: Effect of molecular weight of polyester on the phase and morphology. *Journal of Sol-Gel Science and Technology*, *42*(1), 21–26. https://doi.org/10.1007/s10971-006-1509-3

Satapathy, S., & Wadhawan, V. K. (2005). Fabrication of pyroelectric laser-energy meters and their characterization using Nd: YAG laser of variable pulse-width. *Sensors and Actuators A: Physical*, *121*(2), 576-583. https://doi.org/10.1016/j.sna.2005.04.004

Selbach, S. M., Tybell, T., Einarsrud, M. A., & Grande, T. (2007). Size-dependent properties of multiferroic BiFeO3 nanoparticles. *Chemistry of materials*, *19*(26), 6478-6484. https://doi.org/10.1021/cm071827w

Shiratori, Y., Magrez, A., Fischer, W., Pithan, C., & Waser, R. (2007). Temperature-induced phase transitions in micro-, submicro-, and nanocrystalline NANBO3. *The Journal of Physical Chemistry C*, *111*(50), 18493–18502. https://doi.org/10.1021/jp0738053

Śmiga, W., & Garbarz-Glos, B. (2008). Structural and mechanical properties of ceramic solid solutions Na1-xLixNbO3 for x≤ 0.06. *Ferroelectrics*, *377*(1), 137-145. https://doi.org/10.1080/00150190802523768

Śmiga, W., Garbarz-Glos, B., Antonova, M., Kalvane, A., & Kuś, C. (2009). The Structural and Dielectric Properties of the Li0. 005Na0. 995NbO3 Ceramics. *Ferroelectrics*, *379*(1), 86-93. https://doi.org/10.1080/00150190902850897

Teixeira, G., Gasparotto, G., Paris, E., Zaghete, M., Longo, E., & Varela, J. (2011). Photoluminescence properties of PZT 52/48 synthesized by microwave hydrothermal

method using PVA with template. *Journal of Luminescence*, *132*(1), 46–50. https://doi.org/10.1016/j.jlumin.2011.06.041

Volanti, D. P., Orlandi, M. O., Andrés, J., & Longo, E. (2010). Efficient microwave-assisted hydrothermal synthesis of CuO sea urchin-like architectures via a mesoscale self-assembly. *CrystEngComm*, *12*(6), 1696-1699. https://doi.org/10.1039/D4CE00973H

Xu, G., Jiang, W., Qian, M., Chen, X., Li, Z., & Han, G. (2009). Hydrothermal synthesis of lead zirconate titanate nearly free-standing nanoparticles in the size regime of about 4 nm. *Crystal Growth and Design*, *9*(1), 13-16. https://doi.org/10.1021/cg800287e